

Predictions of unknown masses and their applicationsH. Jiang,^{1,2} G. J. Fu,² B. Sun,³ M. Liu,⁴ N. Wang,⁴ M. Wang,^{5,6} Y. G. Ma,⁷ C. J. Lin,⁸ Y. M. Zhao,^{2,9,*}
Y. H. Zhang,⁵ Zhongzhou Ren,^{9,10} and A. Arima^{2,11}¹*School of Arts and Sciences, Shanghai Maritime University, Shanghai 200135, P.R. China*²*INPAC, Department of Physics and Shanghai Key Lab for Particle Physics and Cosmology, Shanghai Jiao Tong University, Shanghai, 200240, China*³*School of Physics and Nuclear Energy Engineering, Beihang University, Beijing 100191, China*⁴*Department of Physics, Guangxi Normal University, Guilin 541004, China*⁵*Institute of Modern Physics, Chinese Academy of Sciences, Lanzhou 730000, China*⁶*CSNSM-IN2P3, Batiment 104,108, 91405 Orsay Campus, France*⁷*Shanghai Institute of Applied Physics, Chinese Academy of Sciences, Shanghai 201800, China*⁸*Department of Nuclear Physics, China Institute of Atomic Energy, P.O. Box 275(10), Beijing 102413 China*⁹*Center of Theoretical Nuclear Physics, National Laboratory of Heavy Ion Accelerator, Lanzhou 730000, China*¹⁰*Department of Physics, Nanjing University, Nanjing 210093, China*¹¹*Musashi Gakuen, 1-26-1 Toyotamakami Nerima-ku, Tokyo 176-8533, Japan*

(Received 10 February 2012; published 3 May 2012)

In this paper we predict atomic masses which are not experimentally accessible by using local mass relations which connect with the proton-neutron interactions with improved accuracy. Based on our predicted masses, we investigate one-proton and one-neutron drip lines for a few regions in the nuclide chart and α -decay half-lives times for some isotopes with proton number $102 \leq Z \leq 106$. The impact of our predicted one-neutron separation energies on astrophysical r -process nucleosynthesis is discussed within the framework of a classical r -process model.

DOI: [10.1103/PhysRevC.85.054303](https://doi.org/10.1103/PhysRevC.85.054303)

PACS number(s): 21.10.Dr, 21.60.-n, 23.20.Js, 27.90.+b

I. INTRODUCTION

Atomic mass (or binding energy) is a fundamental quantity of a nucleus. It is the key input for theoretical studies on the origin of the heavy elements, especially those on the rapid proton (rp) and rapid neutron (r) capture processes. Although many atomic masses for nuclei close to the β -stability line are measured very accurately, the values of atomic masses remain unknown for a large number of unstable nuclei, due to difficulties in production, separation, and detection.

Describing and predicting atomic masses (or masses for short) have therefore been one of the focuses of nuclear structure physics. Great efforts along this line have been made, with the root-mean-squared deviations (rmsD for short) of several hundred keV to 1 MeV with respect to experimental data [1–30]. Some of these studies are based on microscopic and/or macroscopic mass models; for example, the Duflo-Zuker model (D-Z) [4,5], the finite range droplet model (FRDM) [6,7], the Skyrme-Hartree-Fock-Bogoliubov theory (SHFB) [8–10], the Weizsäcker-Skyrme (WS) mass model [11–14], the Wigner-Kirkwood method [15], and the energy functional with shell-model occupations [16] with the rmsD from 200 to 1300 keV. There are also studies using local nuclear mass relations, such as the Audi-Wapstra systematics [17–19], the Garvey-Kelson (G-K) mass relations [20–27], and the mass relations based on the residual proton-neutron (p - n) interactions [28–30], with the rmsD from 60 to 300 keV. For comprehensive reviews, see Refs. [31,32].

In this paper we improve the accuracy of both the description of the known atomic masses and the prediction of the unknown, and investigate one-proton separation energies S_p , one-neutron separation energies S_n , two-proton separation energies S_{2p} , and two-neutron separation energies S_{2n} . Based on our predicted results, we discuss the proton and neutron drip lines, α -decay energies, and α -decay half-lives for some transuranium nuclei as well as their implications in the r -process nucleosynthesis in the universe.

Our method is an extrapolation approach enlightened by systematics of the proton-neutron (p - n) interactions. These interactions have been realized to play a crucial role in the evolution of collectivity, deformation, and phase transitions [33–37] and were extensively studied in Refs. [38–52]. Assuming empirical values of the p - n interactions, some of the present authors studied local mass relations [28–30]. In this paper we refine our p - n interactions, and make use of the recent experimental database compiled by Audi and Wang [53] in our extrapolations. We predict 1566 atomic masses, 4941 S_p , 6426 S_n , 2457 S_{2p} , and 3960 S_{2n} , with theoretical uncertainties below 1000 keV. The values of theoretical uncertainties are evaluated by the same procedures as in Ref. [30], independently for atomic mass and different types of separation energies.

This paper is organized as follows: In Sec. II we discuss our improvements in both descriptions and predictions of atomic masses and neutron- and proton-separation energies. In Sec. III we investigate one-proton and one-neutron drip lines, and α -decay lifetimes of transuranium nuclei, as well as isotopic abundances under certain astrophysical condition, based on our predicted results. Our summary and conclusion are given in Sec. IV.

* Corresponding author: ymzhao@sjtu.edu.cn

II. PREDICTION OF ATOMIC MASSES

In this paper we take similar conventions as in Refs. [19,53]. For the convenience of readers, we repeat them here. We denote the nuclear mass by M_N , atomic mass by M , proton number by Z , neutron number by N , mass number by $A (= Z + N)$, the total binding energy for Z electrons outside the nucleus by B_e , mass excess by M' , unified atomic mass unit by m_u (one twelfth of the atomic mass of one ^{12}C atom in its electronic and nuclear ground states), and binding energy by $B(N, Z)$. We have

$$\begin{aligned} M_N(Z, N) &= M(Z, N) + ZM_e - B_e, \\ M'(Z, N) &= M(Z, N) - Am_u, \\ B(N, Z) &= ZM_H + NM_n - M(Z, N), \\ S_{ip}(Z, N) &= M(Z - i, N) + iM_H - M(Z, N) \\ &= B(Z, N) - B(Z - i, N), \\ S_{in}(Z, N) &= M(Z, N - i) + iM_n - M(Z, N) \\ &= B(Z, N) - B(Z, N - i). \end{aligned}$$

Here S_{ip} and S_{in} are the i -proton and i -neutron separation energies, respectively. The total p - n interactions (denoted by δV_{ip-jn}) between the last i proton(s) and the last j neutron(s) [40–43] are defined as follows:

$$\begin{aligned} \delta V_{ip-jn}(Z, N) &= S_{ip}(Z, N) - S_{ip}(Z, N - j) \\ &= S_{jn}(Z, N) - S_{jn}(Z - i, N) \\ &= [B(Z, N) - B(Z, N - j)] \\ &\quad - [B(Z - i, N) - B(Z - i, N - j)]. \quad (1) \end{aligned}$$

For $(i, j) = (1, 1), (1, 2), (2, 1)$, the values of δV_{ip-jn} are found to exhibit compact correlations with mass number A and thus are very useful to describe and to predict atomic masses [28–30].

In our extrapolation approach [29,30], it is crucial to evaluate the values of δV_{ip-jn} as accurately as possible. In Ref. [30] δV_{ip-jn} was assumed to take the average value of $\delta V_{ip-jn}(A)$ [denoted by $\overline{\delta V_{ip-jn}(A)}$] with a number of corrections (the shell effect, the Coulomb correction, the symmetry energy correction) among which the dominant correction is called the shell correction. In this work, instead of considering all these corrections, we focus on the dominant shell correction. We assume free parameters of the shell correction for each shell. We denote our evaluated δV_{ip-jn} by using $\delta V_{ip-jn}^{\text{cal}}$ and have

$$\begin{aligned} -\delta V_{1p-1n}^{\text{cal}}(Z, N) &= -\overline{\delta V_{1p-1n}}(A) + \Delta_{\text{sh}}(Z, N), \\ -\delta V_{1p-2n}^{\text{cal}}(Z, N) &= -\overline{\delta V_{1p-2n}}(A) + \Delta_{\text{sh}}(Z, N) \\ &\quad + \Delta_{\text{sh}}(Z, N - 1), \\ -\delta V_{2p-1n}^{\text{cal}}(Z, N) &= -\overline{\delta V_{2p-1n}}(A) + \Delta_{\text{sh}}(Z, N) \\ &\quad + \Delta_{\text{sh}}(Z - 1, N), \quad (2) \end{aligned}$$

where

$$\begin{aligned} \Delta_{\text{sh}}(Z, N) &= a_{\text{sh}} + 2b_{\text{sh}}|\delta_p \Omega_N(N_p - \Omega_Z) \\ &\quad - \delta_n \Omega_Z(N_n - \Omega_N)| \quad (3) \end{aligned}$$

is called the shell correction term, introduced in Ref. [30]. The shell effect on residual proton-neutron interactions was

TABLE I. The parameters [in keV, see Eq. (3)] taken in this work for different mass regions. These parameters are obtained via a χ^2 fitting procedure.

Region	Parameter	Even- A	Odd- A
$Z \in [1, 28), N \in [1, 28)$	a_{sh}	28.55	136.7
	b_{sh}	-0.3958	-5.138
$Z \in [1, 28), N \in [28, 50)$ or $Z \in [28, 50), N \in [1, 28)$	a_{sh}	7.372	45.74
	b_{sh}	-0.628	-0.1966
$Z \in [28, 50), N \in [28, 50)$	a_{sh}	141.3	-177.2
	b_{sh}	-0.6086	0.8863
$Z \in [28, 50), N \in [50, 82)$ or $Z \in [50, 82), N \in [28, 50)$	a_{sh}	59.26	7.282
	b_{sh}	-0.2223	-0.0007
$Z \in [50, 82), N \in [50, 82)$ or $Z \in [28, 50), N \in [82, 126)$	a_{sh}	129.2	-84.88
	b_{sh}	-0.2666	0.1337
$Z \in [50, 82), N \in [82, 126)$ or $Z \in [82, 126), N \in [50, 82)$	a_{sh}	60.64	107.9
	b_{sh}	-0.1124	-0.2617
$Z \in [82, 126), N \in [82, 126)$ or $Z \in [50, 82), N \in [126, 184)$	a_{sh}	11.37	18.81
	b_{sh}	-0.1067	-0.0266
$Z \in [82, 126), N \in [126, 184)$	a_{sh}	44.67	-11.25
	b_{sh}	-0.1697	0.0499

discussed in Refs. [46,47,50], where it was shown that proton-neutron interactions are stronger if the proton fractional fillings and neutron fractional fillings are close to each other [52]. The form of our shell correction Δ_{sh} is enlightened by this feature. Here N_p (N_n) is the valence proton (neutron) number with respect to the nearest closed shell, δ_p (δ_n) equals $+1$ if the valence protons (neutrons) are particle-like and -1 if are hole-like, $\Omega_Z = \sum_{j_Z} (j_Z + \frac{1}{2})$ where j_Z represents spin of single-particle levels for valence protons, and similarly $\Omega_N = \sum_{j_N} (j_N + \frac{1}{2})$ where j_N represents spin of single-particle levels for valence neutrons. There are two shell-correction terms in both $\delta V_{1p-2n}^{\text{cal}}$ and $\delta V_{2p-1n}^{\text{cal}}$, because these two types of p - n interactions can be decomposed into two terms of $\delta V_{1p-1n}^{\text{cal}}$ [30].

The parameters a_{sh} and b_{sh} are adjusted for each shell to optimize the agreement between the calculated $\delta V_{ip-jn}^{\text{cal}}$ based on Eq. (2) and δV_{ip-jn} evaluated from Eq. (1). Our a_{sh} and b_{sh} are shown in Table I, where one sees that, for different shells, their values change drastically. They are also very different from those if one uses only one unified set of parameters (see Table I of Ref. [30]) for all shells. Such change suggests that the role played by the shell closures on $\delta V_{ip-jn}^{\text{cal}}(N, Z)$ is complicated and very different in different regions.

Table II compares the rmsDs (in keV) of our $\delta V_{ip-jn}^{\text{cal}}$ evaluated by Eq. (2) with those extracted by using experimental masses. We also list the rmsD values of $\delta V_{ip-jn}^{\text{cal}}$ evaluated in Ref. [30]. One sees the values of $\delta V_{ip-jn}^{\text{cal}}$ in this work are refined in comparison with those in Ref. [30]. For mass number $A \geq 16$, the rmsD between our calculated δV_{ip-jn} and those extracted by using experimental masses is reduced by ~ 21 to 29 keV.

Replacing δV_{ip-jn} [(i, j) = (1, 1), (1, 2), (2, 1)] in Eq. (1) by using $\delta V_{ip-jn}^{\text{cal}}$ evaluated by using Eq. (2), we obtain a number of ways to evaluate the binding energies, one- or two-proton, and one- or two-neutron separation energies. For simplicity we leave these formulas in the appendix [the formulas of predicting binding energies are the same as Eqs. (9) and (10)

TABLE II. The rmsDs (in keV) of our calculated $\delta V_{ip-jn}^{\text{cal}}$ in comparison with those extracted by experimental data of binding energies compiled in Ref. [53]. For comparison we list the rmsD of our $\delta V_{ip-jn}^{\text{cal}}$ calculated in Ref. [30].

	Region	δV_{1p-1n}	δV_{1p-2n}	δV_{2p-1n}
This work	$A \geq 16$	184	213	220
	$A \geq 60$	142	150	163
	$A \geq 120$	121	129	141
Ref. [30]	$A \geq 16$	213	235	241
	$A \geq 60$	159	168	175
	$A \geq 120$	124	134	142

of Ref. [30], and thus are omitted in this paper]. Similar to Refs. [24–30], we take the average of all possible $B^{\text{pred}}(N, Z)$, $[S_p^{\text{pred}}(Z, N), S_n^{\text{pred}}(Z, N), S_{2p}^{\text{pred}}(Z, N), \text{ and } S_{2n}^{\text{pred}}(Z, N)]$ for a given nucleus. The uncertainty of our predicted results is calculated by the same method as in Ref. [30].

Before going to our predicted results, it is worth taking a look at the accuracy of our description for known masses. In Table III we show the rmsDs of our calculated masses in comparison with experimental values in the database compiled in Ref. [53]. The results obtained in Refs. [29,30] and those by using the Garvey-Kelson relations are also presented. One sees the substantial improvement of the accuracy in describing the known masses in the present work.

Our predicted masses usually have small uncertainties; in particular for cases when the number of equations to evaluate the mass for a given nucleus is larger than one, the uncertainties of our predicted masses are sometimes smaller than those of the experimental data. In such cases we replace such experimental values by using our predicted results and find improvements in extrapolating the AME2003 database [19] to predict unknown masses. In Table IV we show the results of a numerical experiment: We calculate the rmsDs (in keV) of our predicted masses based on the AME2003 database [19] with respect to the new experimental data (151 nuclei) compiled in Ref. [53]. In one set of predictions, we assume all experimental data compiled in Ref. [19]; in another set of predictions, we replace experimental data by using our predicted results which have smaller uncertainties; that is, when the experimental uncertainties are larger than those of our predicted results, we replace these experimental data by our predicted results.

TABLE III. rmsDs (in keV) of our predicted masses and experimental results compiled in Ref. [53]. For comparison we present the rmsDs of predicted masses by using the G-K relations (2nd row) of Ref. [25], the rmsDs obtained in Refs. [29,30] (3rd and 4th rows), for nuclei with $A \geq 60$. n is the number of possible evaluations for a given nucleus.

Relations	$n \geq 1$	$n \geq 4$	$n \geq 7$	$n \geq 8$	$n \geq 12$
This work	89	80	73	72	67
G-K	115	98	86		76
Ref. [29]	123	92	73	70	
Ref. [30]	107				

TABLE IV. The rmsDs (in keV) of our predicted masses based on the AME2003 database [19] with respect to the new data (151 nuclei) compiled in Ref. [53]. Pred-1 assumes the experimental data compiled in Ref. [19], and Pred-2 replaces experimental data by our predicted results for which our predicted results have smaller uncertainties. Pred-3 correspond to the rmsDs of the predicted results in the AME2003 database [19] in comparison with new experimental data compiled in Ref. [53]. One sees smaller rmsDs in Pred-2, which means that one achieves more accurate predicted results if one replaces experimental masses by our predicted results for those with smaller uncertainties. See text for details.

Region	Pred-1	Pred-2	Pred-3
$A \geq 16$	400	387	400
$A \geq 60$	398	385	391
$A \geq 120$	204	204	262

One sees that one obtains sizable improvements in doing so in Table IV.

It is also worth addressing some cases for which previously predicted masses in Ref. [30] exhibit large deviations from recent experimental data compiled in Ref. [53]. In Fig. 4 of Ref. [30], predicted masses for ^{85}Mo , $^{87-89}\text{Tc}$, ^{123}Ag , ^{140}I , ^{222}Po , $^{226-228}\text{Rn}$, $^{233,234}\text{Ra}$, and ^{235}Ac have large deviations from experimental data. For ^{85}Mo , $^{87-89}\text{Tc}$, and ^{123}Ag , the results could be improved by using the new experimental data in Refs. [51,54–56,63]; but for ^{140}I , ^{222}Po , $^{226-228}\text{Rn}$, $^{233,234}\text{Ra}$, and ^{235}Ac , the deviations are large due to the overestimation of p - n interactions [30]. In this paper all these experimental results are well reproduced, as shown in Fig. 1.

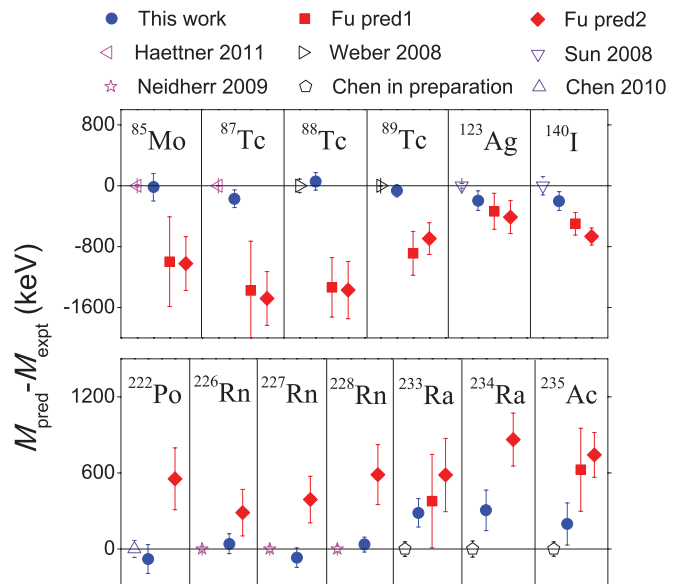


FIG. 1. (Color online) Deviations of our predicted masses (denoted by M_{pred} , solid blue circles, in unit of keV) from experimental data M_{expt} (open symbols). The red symbols are taken from Ref. [30] (denoted by Fu Pred1, Fu Pred2). The experimental results include Haettner 2011 [54], Weber 2008 [55], Sun 2008 [56], Neidherr 2009 [57], Chen in preparation [58], and Chen 2010 [59].

	14	15	16	17	18	19	20	21	22	23	24	25	26	27	28	
28				-3.33(39)	-1.63(53)	-1.40(35)	-0.14(45) -0.39(67)	+0.08(31) +0.49(57)	+1.05(37) +1.31(40)	+1.41(26) +1.62(34)	+2.38(26) +2.90(25)	+2.95(20) +3.06(31)	+4.08(26) <i>+3.85(5)</i>	+4.39(25) <i>+4.61(0)</i>	+6.90(20) <i>+7.17(0)</i>	Ni
				-8.40(83)	-6.22(77)	-4.32(72)	-2.73(66) -2.68(40)	-1.32(60) -0.75(48)	-0.20(53) +0.01(31)	+1.21(46) +1.28(33)	+2.42(37) +2.98(21)	+3.86(27) +4.04(30)	+5.47(5)	+8.97(0)	+12.10(25) <i>+12.23(0)</i>	
27						-2.83(41)	-2.81(49) -2.31(54)	-1.32(36) -1.24(48)	-1.25(39) -1.30(27)	-0.25(32) -0.34(22)	+0.03(27) +0.08(16)	+1.17(30) +0.98(7)	+1.61(1)	+4.53(22) <i>+4.35(0)</i>		Co
							-1.01(64) -0.89(50)	+0.32(57) +0.70(42)	+1.73(42) +1.89(31)	+2.87(36) +2.45(20)	+4.19(28) +4.24(15)	+6.05(30) +5.87(7)	+8.99(0)	+12.36(32) <i>+11.88(0)</i>		
26				-2.02(38)	-0.40(49)	-0.12(33) +0.18(54)	+1.56(39) +1.42(46)	+1.76(28) +1.94(28)	+2.95(28) +3.19(17)	+3.30(21) +2.79(19)	+4.46(27) <i>+4.16(6)</i>	+4.59(27) <i>+4.88(2)</i>	+7.21(21) <i>+7.38(1)</i>			Fe
				-5.69(77)	-3.70(70)	-1.84(64) <i>-1.15(1)</i>	+0.20(56) +0.68(40)	+1.98(49) +1.79(33)	+3.51(39) +3.27(7)	+4.91(29) +4.84(15)	+4.91(29) <i>+6.24(6)</i>	+9.47(2)	+12.59(26) <i>+12.65(1)</i>			
25				-3.24(62)	-2.95(38)	-1.25(50) -1.34(54)	-1.20(31) -0.74(36)	+0.58(36) -0.15(23)	+0.66(23) +0.08(16)	+1.89(30) <i>+2.05(11)</i>	+2.25(29) <i>+2.08(3)</i>	+4.98(24) <i>+4.58(0)</i>				Mn
				-4.27(81)	-2.39(72)	-0.51(65) +0.31(71)	+1.24(55) +1.67(38)	+3.33(46) +2.42(17)	+5.20(31) +4.96(16)	+6.83(11) <i>+10.19(2)</i>	+13.39(35) <i>+12.73(0)</i>					
24			-0.71(52)	-0.51(35)	+1.11(42) +0.77(36)	+1.23(30) +1.64(54)	+2.99(29) +2.41(30)	+2.96(23) +2.58(23)	+4.55(29) <i>+4.88(3)</i>	+5.10(28) <i>+4.77(1)</i>	+8.12(22) <i>+8.10(1)</i>					Cr
			-4.69(75)	-2.80(69)	-1.05(60) -0.77(34)	+0.73(52) +1.43(41)	+2.49(42) +2.62(20)	+4.32(30) +4.66(20)	+6.50(2) <i>+10.13(1)</i>	+13.50(28) <i>+13.27(0)</i>						
23			-3.04(41)	-1.41(54) -2.11(69)	-1.45(54) -1.53(26)	+0.30(39) -0.22(62)	+0.05(24) +0.21(23)	+1.37(32) <i>+2.08(12)</i>	+2.33(31) <i>+1.62(2)</i>	+5.11(26) <i>+5.36(0)</i>						V
			-2.45(79)	-0.56(71) -1.41(54)	+1.22(60) +0.43(21)	+2.86(50) +1.64(50)	+4.53(34) +3.96(23)	+6.57(12) <i>+10.27(2)</i>	+13.56(38) <i>+13.84(0)</i>							
22	-2.07(49)	-1.48(35)	-0.09(36) +0.28(50)	+0.57(29) +0.70(36)	+1.93(31) <i>+1.97(16)</i>	+2.29(21) <i>+1.86(36)</i>	+3.62(26) <i>+3.75(0)</i>	+4.08(30) <i>+4.49(1)</i>	+8.30(24) <i>+8.65(0)</i>							Ti
	-6.07(70)	-4.33(61)	-2.41(50) -2.52(40)	-0.42(38) -0.71(30)	+0.72(49) <i>+1.37(16)</i>	+3.17(27) <i>+2.38(36)</i>	+3.92(48) <i>+4.84(0)</i>	+13.27(30) <i>+8.76(0)</i>	+13.58(0) <i>+13.58(0)</i>							
21		-2.92(42) -3.47(36)	-2.42(36) -2.80(30)	-1.22(32) -1.41(20)	-0.69(26) -0.60(22)	+0.96(30) <i>+0.53(0)</i>	+0.74(25) <i>+1.09(0)</i>	+4.51(29) <i>+4.27(0)</i>								Sc
	-3.43(78)	-1.58(69) -2.19(42)	+0.05(54) -0.23(30)	+2.05(40) +1.60(20)	+4.24(37) <i>+3.95(2)</i>	+6.02(43) <i>+6.30(0)</i>	+9.41(0)	+13.28(41) <i>+13.16(0)</i>								
20	+0.85(36) +0.48(36)	+1.26(28) +1.28(36)	+2.58(28) <i>+2.57(4)</i>	+3.22(22) <i>+3.01(0)</i>	+4.71(24) <i>+4.55(0)</i>	+5.19(26) <i>+5.77(0)</i>	+8.81(26) <i>+5.77(0)</i>									Ca
-1.20(52) -1.47(30)	+0.68(38) +0.41(20)	+2.94(36) <i>+2.63(4)</i>	+4.33(29) <i>+4.67(0)</i>	+6.80(34) <i>+6.40(0)</i>	+14.91(33) <i>+10.91(0)</i>	+14.71(0)										

FIG. 2. (Color online) Predicted one- and two-proton separation energies (S_p and S_{2p} , in MeV) for $N \sim Z$ nuclei with proton number Z from 20 to 28. In each of the blocks the first row corresponds to S_p predicted in this work, the second row correspond to S_p in Ref. [53], the third row corresponds to S_{2p} in this work, and the fourth row corresponds to S_{2p} in Ref. [53]. The predicted results and experimental data in Ref. [53] are in normal and italic, respectively. The dashed line in each block are plotted to guide eyes. The line in red plots the one-proton drip line predicted in this work.

We close this section by addressing why our extrapolation approach works well in describing and predicting atomic masses. First, the p - n interactions that we exploit include $1n$ - $1p$, $2n$ - $1p$, and $1n$ - $2p$ types. On the one hand, these interactions have been much less investigated than the $2n$ - $2p$ -type proton-neutron interactions (i.e., $\delta V_{2p-2n}^{\text{cal}}$), and have been much less known. On the other hand, they exhibit remarkable systematics with respect to mass number A . In particular, $1n$ - $1p$ -type (generally speaking, ip - jn type with ij odd) p - n interactions were found to have an odd-even effect which is given dominantly by the pairing interaction [30,38,64]. The results of $\delta V_{1p-1n}^{\text{cal}}$ for both even- A and odd- A nuclei lie within a very compact envelope of points. Second, most extrapolation approaches assume that the one- and two-body interactions evolve very slowly and are thus assumed to be constants in local regions. In our approach, we go one step forward: we refine the systematics of two-body interactions (here p - n interactions) by considering the shell effect. These refined p - n interactions therefore provide us with local mass relations which have smaller rmsD values. Third, if the number of ways to predict the mass of a given nucleus is more than one, our predicted value is given by the average values of all predictions. Such an advantage was first pointed out by Barea *et al.* in Refs. [24,25] for the Garvey-Kelson relations. The reason why averaging the predicted results reduces the deviations from experimental values has not yet been well understood. One possible origin might be that some of the white noises arising in many-body correlations are canceled out with each other in averaging the

predictions and that such cancellation reduces the rmsD in our predictions.

III. APPLICATION OF OUR PREDICTED MASSES

In this section we make use of these results to investigate the proton and neutron drip lines, α -decay lifetimes for heavy nuclei, and the impact on the astrophysical r -process simulations.

A. Proton and neutron drip lines

We first come to the proton drip line. In Figs. 2 and 3 we present our predicted results for one- and two-proton separation energies (S_p and S_{2p}) of nuclei with proton number from 20 to 38, close to the proton drip line. In each of the blocks the first row correspond to S_p predicted in this work, the second row corresponds to S_p in Ref. [53], the third row corresponds to S_{2p} in this work, and the fourth row corresponds to S_{2p} in Ref. [53]. The available experimental data compiled in Ref. [53] are in italic. The line in red is our predicted one-proton drip line. We list here a few nuclei with negative [but very small in magnitude] one-proton separation energies: ^{39}Sc , ^{38}Ti , ^{42}V , ^{41}Cr , ^{50}Co , $^{54,55}\text{Cu}$, $^{54,55}\text{Zn}$, $^{58,59}\text{Ge}$, ^{64}As , $^{62,63}\text{Se}$, $^{68,69}\text{Br}$, $^{66,67}\text{Kr}$, $^{72,73}\text{Rb}$, and $^{70,71}\text{Sr}$. These nuclei are good candidates for one-proton emissions.

In Figs. 2 and 3 one sees that the agreement between our predicted results and those given in Ref. [53] is very good in general. However, we should also point out a few cases

	23	24	25	26	27	28	29	30	31	32	33	34	35	36	37	38	
38						-2.70(33)	-2.72(48)	-1.57(30)	-1.62(42)	-0.33(27)	-0.37(37)	+0.85(26)	+0.86(30)	+2.16(29)	+1.99(22)	+4.70(15)	Sr
													+1.12(64)	+2.04(14)	+4.32(3)		
													+0.20(42)	+1.47(10)	+4.64(22)	+6.93(13)	
37																+2.40(16)	Rb
																+2.65(1)	
																+7.14(16)	
																+7.43(1)	
36				-2.76(32)	-2.57(46)	-1.33(29)	-1.38(40)	-0.02(26)	-0.10(33)	+1.09(24)	+0.97(25)	+2.29(24)	+2.40(39)	+2.19(13)	+4.75(16)		Kr
											+0.99(51)	+2.40(39)	+2.19(13)	+4.73(1)			
											+0.43(41)	+1.95(38)	+4.60(13)	+6.68(13)	+6.59(1)		
35																	Br
34		-3.66(33)	-3.28(47)	-2.18(30)	-1.96(40)	-0.63(26)	-0.54(33)	+0.69(23)	+0.58(23)	+1.96(22)	+1.96(22)	+1.84(7)	+4.91(17)				Se
								+0.69(71)	+0.86(67)	+2.07(31)	+1.84(7)	+4.89(0)					
								-0.50(40)	+0.64(28)	+1.87(24)	+1.98(30)	+4.69(7)					
								-0.74(52)	+0.58(60)	+1.98(30)	+4.69(7)	+7.16(0)					
33																	As
32																	Ge
31																	Ga
30																	Zn
29																	Cu

FIG. 3. (Color online) Same as Fig. 2 except for proton number from 29 to 38. The unit of separation energies is MeV.

with sizable disagreements in comparison to other studies. Reference [60] predicted S_p and S_{2p} for proton-rich nuclei in the region $A = 41$ to 75 based on Skyrme Hartree-Fock calculations. It is noted that most of our predicted S_{2p} are close to those obtained in Ref. [60] except for ^{54}Cu , $^{54-56}\text{Zn}$, and ^{58}Ge (deviations are larger than 500 keV). For ^{54}Zn , our predicted $S_{2p} = -2.49(57)$ MeV, almost two times of that in Ref. [60] [$-1.33(14)$ MeV], which is well consistent with experimental data $-1.48(2)$ MeV [65] and $-1.28(21)$ MeV [66]. It would be therefore worth investigating why extrapolations in this work and Ref. [53] fail in predicting the mass of ^{54}Zn in future studies.

In Figs. 2 and 3 there are a few nuclei (with $N = Z$, $Z - 1$, or $Z - 2$; e.g., $^{61}\text{Ga}_{30}$) for which we are unable to predict reasonably their S_p and/or S_{2p} . We leave such S_p and S_{2p} blank in Figs. 2 and 3. This situation mainly originates from the anomaly of $\delta V_{1p-1n}(Z, N)$ with $Z = N$. We discard these exceptionally large $\delta V_{1p-1n}(Z, N)$ [for the same reason, $\delta V_{1p-2n}(Z, N)$ with $Z = N$ or $Z = N - 1$, and $\delta V_{2p-1n}(Z, N)$ with $Z = N$ or $Z = N + 1$] in our predictions; see Ref. [30] for more details. For a few cases (e.g., $^{58,59}\text{Zn}$), however, we are able to obtain S_p and S_{2p} by using our predicted binding energies of their neighboring nuclei.

In Fig. 4 we show the one-proton-drip line nuclei with $20 \leq Z \leq 38$, $51 \leq Z \leq 72$, $73 \leq Z \leq 91$, and $92 \leq Z \leq 106$, and compare them with results of previous studies (including experimental results) [60–62]. One sees that all these models give similar predictions of the one-proton drip line. This is partly due to the situation that current experimental measurements are approaching the proton drip line in a number of regions.

In Fig. 5 we plot our predicted one-neutron separation energy versus neutron number N for Ca, Ni, Sn, and Tm isotopes and compare with results from previous works. All these studies predict similar patterns, although there are small differences for large- N cases. Scrutinizing more carefully, however, one sees that the results in this work and predictions in Ref. [53] are in better agreement with experimental data than other works [and our prediction goes further]. According to this work, the one-neutron drip line nuclei for Ca, Ni, and Sn isotopes with odd neutron numbers are ^{59}Ca , ^{81}Ni , and ^{153}Sn , respectively; for the same isotopes with even neutron numbers, our predicted one-neutron drip line nuclei are ^{70}Ca , ^{94}Ni , and ^{174}Sn , respectively. In Ref. [67], ^{72}Ca , ^{98}Ni , and ^{176}Sn are one-neutron drip line nuclei, based on the relativistic continuum Hartree-Bogoliubov (RCHB) theory. According to Ref. [68] ^{59}Ca and ^{97}Ni are one-neutron drip line nuclei.

In Figs. 6 and 7, we present the one- and two-neutron separation energies (S_n and S_{2n}) for neutron-drip nuclei with proton number $Z = 29$ to 38. Our predicted neutron drip line exhibits a drastic odd-even staggering (much more drastic than that for proton drip line, as shown in Figs. 2 and 3). For example, our predicted one-neutron drip line nucleus with $Z = 30$ is ^{93}Zn for odd N , and ^{104}Zn for even N .

B. Transuranium nuclei

In this subsection we discuss the masses of transuranium nuclei, their α -decay energies (Q_α) and half-lives of α -decays.

We first come to our predicted masses. There are 134 nuclei with available experimental data in this region, according to

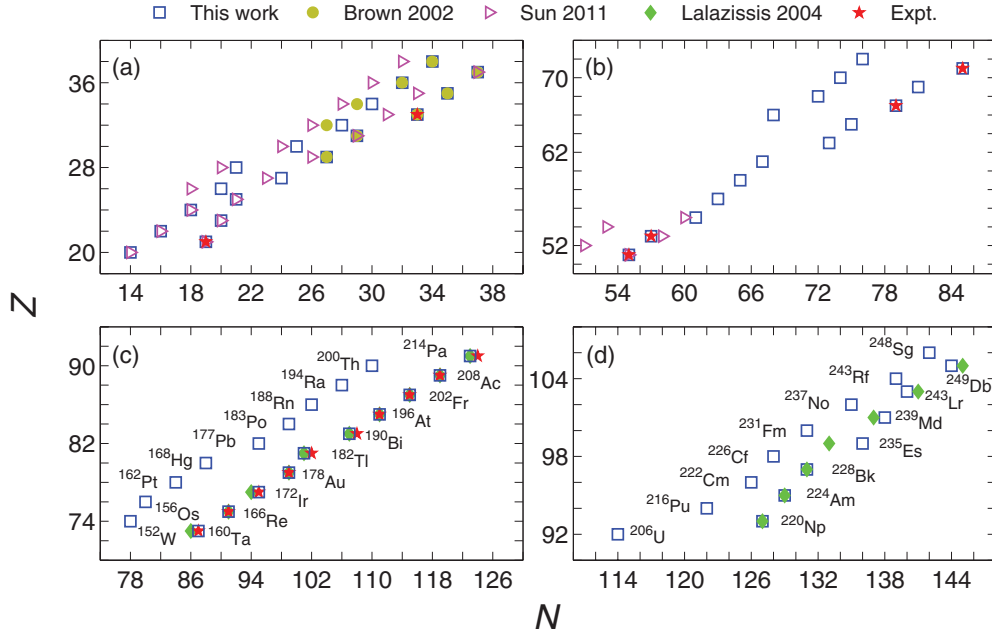


FIG. 4. (Color online) One-proton drip-line nuclei (i.e., those with positive S_p values which would be negative if one more proton were added): (a) $20 \leq Z \leq 38$, (b) $51 \leq Z \leq 72$, (c) $73 \leq Z \leq 91$, (d) $92 \leq Z \leq 106$. The open squares in blue are our predicted results, others are taken from previous studies: Brown 2002 [60], Sun 2011 [61], Lalazissis 2004 [62], and experimental (Expt) [53].

Ref. [53]. For these nuclei the rmsD of our predicted masses with respect to the experimental results is only ~ 50 keV. Such small deviation demonstrates the high accuracy of our evaluated p - n interactions in this region. Because experimental masses in this region are relatively scarce, for those which are

not accessible in the experimental database, we assume that

$$-\overline{\delta V_{1p-1n}}(A) = \begin{cases} 74 \text{ keV} & \text{odd } A \\ 74 + \frac{69861}{A} \text{ keV} & \text{even } A, \end{cases}$$

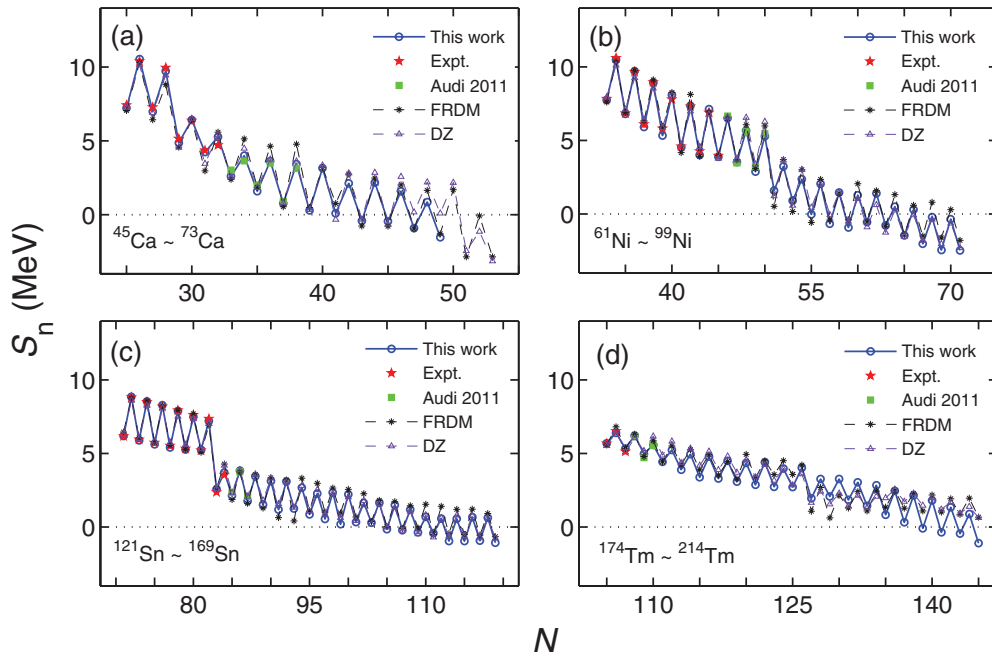


FIG. 5. (Color online) One-neutron separation energies (S_n , in MeV) versus neutron number N : (a) Ca, (b) Ni, (c) Sn, (d) Tm. Our predicted results are shown as open circles in blue, experimental results are taken from Ref. [53]. Results of other works (Audi 2011, FRDM, DZ) are taken from Refs. [53], [6], and [4,5], respectively.

	53	55	57	59	61	63	65	67	69	71	73	75	77	79	81	83	
38	+5.80(10) +5.77(1)	+5.30(10) +5.29(1)	+4.47(10) +4.35(1)	+3.66(10) +3.73(1)	+3.78(10) +4.16(1)	+3.48(16) +3.80(8)	+2.96(16) +3.21(29)	+2.33(17) +2.76(64)	+1.77(18) +1.47(28)	+0.80(20) +0.71(22)	+0.71(22) +0.76(22)	+0.41(33) +0.99(23)	+0.99(23) +0.99(23)	+0.99(23) +0.99(23)	+0.99(23) +0.99(23)	+0.99(23) +0.99(23)	Sr
	+13.66(13) +13.59(1)	+12.65(13) +12.58(1)	+11.09(13) +11.18(1)	+9.56(13) +9.61(1)	+9.93(13) +10.08(1)	+9.17(19) +9.18(8)	+8.13(25) +8.11(21)	+6.99(30) +7.22(54)	+6.04(35) +5.30(39)	+4.48(41) +4.08(45)	+4.08(45) +4.08(48)	+3.42(47) +3.63(48)	+3.63(48) +3.63(48)	+3.63(48) +3.63(48)	+3.63(48) +3.63(48)	+3.63(48) +3.63(48)	
37	+5.67(12) +5.72(1)	+5.02(12) +5.10(1)	+4.20(12) +4.01(1)	+3.52(13) +3.53(2)	+3.54(13) +3.58(5)	+3.63(19) +3.40(23)	+2.82(17) +2.99(37)	+2.17(26) +2.99(37)	+1.66(29) +2.22(39)	+1.37(21) +4.46(43)	+0.71(32) +3.61(44)	+0.62(35) +3.25(48)	+0.60(37) +3.24(50)	+0.32(23) +2.67(50)	+0.86(37) +2.84(51)	+1.10(37) +0.84(50)	Rb
	+12.77(15) +12.90(1)	+11.57(15) +11.55(1)	+10.20(14) +9.93(1)	+8.88(14) +8.94(0)	+8.72(15) +8.82(5)	+8.21(19) +8.66(20)	+7.24(29) +7.49(36)	+6.13(34) +6.13(34)	+5.22(39) +5.22(39)	+4.46(43) +4.46(43)	+3.61(44) +3.61(44)	+3.25(48) +3.25(48)	+3.24(50) +3.24(50)	+2.67(50) +2.67(50)	+2.84(51) +2.84(51)	+0.84(50) +0.84(50)	
36	+4.99(10) +4.92(0)	+4.15(10) +4.09(0)	+3.32(11) +3.44(0)	+2.85(13) +2.88(2)	+3.09(13) +2.42(13)	+2.86(18) +2.37(71)	+2.13(23) +2.37(71)	+1.47(20) +2.37(71)	+0.98(21) +4.41(42)	+0.67(32) +3.64(45)	-0.05(22) +2.76(47)	-0.11(24) +2.46(50)	-0.07(24) +2.50(52)	-0.32(36) +1.94(52)			Kr
	+12.16(13) +11.97(0)	+10.46(13) +10.58(0)	+9.19(13) +9.30(0)	+8.05(17) +8.17(2)	+7.98(17) +7.41(13)	+7.16(25) +7.48(52)	+6.33(33) +6.33(33)	+5.33(36) +5.33(36)	+4.41(42) +4.41(42)	+3.64(45) +3.64(45)	+2.76(47) +2.76(47)	+2.46(50) +2.46(50)	+2.50(52) +2.50(52)	+1.94(52) +1.94(52)			
35	+4.85(12) +4.90(0)	+4.02(14) +3.80(0)	+3.20(15) +3.20(0)	+2.66(14) +2.82(45)	+2.83(16) +2.52(78)	+2.55(19) +2.52(78)	+1.91(20) +2.52(78)	+1.35(31) +2.52(78)	+0.81(33) +4.47(41)	+0.56(23) +3.57(45)	-0.15(36) +2.84(48)	-0.21(39) +1.95(50)	-0.17(40) +1.62(53)				Br
	+11.03(15) +11.23(0)	+9.64(15) +9.43(0)	+8.34(19) +8.38(1)	+7.16(18) +7.51(40)	+6.49(22) +6.89(72)	+6.24(31) +6.24(31)	+5.36(37) +5.36(37)	+4.47(41) +4.47(41)	+3.57(45) +3.57(45)	+2.84(48) +2.84(48)	+1.95(50) +1.95(50)	+1.62(53) +1.62(53)	+1.69(55) +1.69(55)				
34	+3.99(11) +3.99(0)	+3.14(13) +3.18(1)	+2.43(13) +2.48(64)	+1.89(17) +2.06(100)	+2.20(21) +2.06(100)	+1.95(25) +5.59(28)	+1.21(28) +5.41(35)	+0.63(22) +4.33(41)	+0.14(23) +3.58(44)	-0.07(35) +2.79(48)	-0.85(24) +2.06(51)	-0.94(25) +1.16(52)					Se
	+10.31(14) +10.16(0)	+8.57(16) +8.71(0)	+7.43(17) +7.49(50)	+6.25(25) +6.52(95)	+5.59(28) +5.59(28)	+5.41(35) +5.41(35)	+4.33(41) +4.33(41)	+3.58(44) +3.58(44)	+2.79(48) +2.79(48)	+2.06(51) +2.06(51)	+1.16(52) +1.16(52)	+0.79(55) +0.79(55)					
33	+3.95(14) +3.84(0)	+2.98(15) +3.34(40)	+2.23(19) +2.46(78)	+1.73(19) +2.16(92)	+1.95(19) +4.58(33)	+1.74(21) +4.50(39)	+0.88(22) +3.44(45)	+0.42(36) +2.63(48)	+0.02(37) +1.95(51)	-0.23(25) +1.24(54)	-0.97(40) +0.38(55)						As
	+9.21(15) +9.25(0)	+7.66(19) +8.07(40)	+6.54(26) +6.59(72)	+5.26(31) +5.79(92)	+4.58(33) +4.58(33)	+4.50(39) +4.50(39)	+3.44(45) +3.44(45)	+2.63(48) +2.63(48)	+1.95(51) +1.95(51)	+1.24(54) +1.24(54)	+0.38(55) +0.38(55)						
32	+2.88(14) +3.05(0)	+2.16(18) +2.55(64)	+1.51(18) +1.68(106)	+0.93(24) +4.31(36)	+1.21(27) +3.67(38)	+1.08(30) +3.62(43)	+0.32(32) +2.63(48)	-0.29(24) +1.63(50)	-0.68(25) +1.09(53)	-0.86(39) +0.49(56)							Ge
	+8.17(18) +8.29(0)	+6.68(26) +7.26(50)	+5.66(31) +5.76(95)	+4.31(36) +4.31(36)	+3.67(38) +3.67(38)	+3.62(43) +3.62(43)	+2.63(48) +2.63(48)	+1.63(50) +1.63(50)	+1.09(53) +1.09(53)	+0.49(56) +0.49(56)							
31	+2.83(16) +3.10(40)	+2.02(19) +2.30(86)	+1.32(27) +4.59(37)	+0.79(21) +3.41(40)	+1.05(22) +2.70(42)	+0.86(23) +2.63(47)	+0.10(24) +1.74(51)	-0.64(40) +0.76(53)	-0.89(41) +0.16(56)								Ga
	+7.12(20) +7.50(40)	+5.55(33) +6.32(81)	+4.59(37) +4.59(37)	+3.41(40) +3.41(40)	+2.70(42) +2.70(42)	+2.63(47) +2.63(47)	+1.74(51) +1.74(51)	+0.76(53) +0.76(53)	+0.16(56) +0.16(56)								
30	+1.94(19) +6.01(27)	+1.07(26) +4.45(38)	+0.44(21) +3.61(41)	+0.07(30) +2.55(44)	+0.29(32) +1.78(45)	+0.12(34) +1.75(50)	-0.52(37) +0.89(54)	-1.19(27) -0.03(56)									Zn
	+6.68(50) +1.74(20)	+4.45(38) +0.92(22)	+3.61(41) +0.29(33)	+2.55(44) -0.08(24)	+1.78(45) +0.14(25)	+1.75(50) -0.03(25)	+0.89(54) -0.74(26)	-0.03(56) -0.03(56)									
29	+4.97(34)	+3.27(43)	+2.49(45)	+1.51(48)	+0.91(49)	+0.80(53)	+0.07(57)		Cu								

One-neutron drip line
for odd neutron number

FIG. 6. (Color online) One- and two-neutron separation energies (in MeV) of neutron-rich nuclei with odd neutron numbers, while proton numbers Z change from 29 to 38. Similar to Figs. 2 and 3 in that each of the blocks in the first row corresponds to S_n , predicted in this work, the second row corresponds to S_n predicted in Ref. [53], the third row corresponds to S_{2n} in this work, and the fourth row corresponds to S_{2n} in Ref. [53]. The predicted results and experimental data of Ref. [53] are in normal and italic, respectively. The line in red plots the one-neutron drip line predicted in this work.

and

$$\begin{aligned} -\overline{\delta V_{1p-2n}}(A) &= 23040A^{-0.67} - 170 \text{ keV}, \\ -\overline{\delta V_{2p-1n}}(A) &= 26560A^{-0.72} - 92 \text{ keV}. \end{aligned} \quad (4)$$

The assumption for $\overline{\delta V_{1p-1n}}(A)$ was given in Ref. [30], and the assumption for $\overline{\delta V_{1p-2n}}(A)$ and $\overline{\delta V_{2p-1n}}(A)$ is given in this work. Both assumptions are empirically obtained based on systematics of proton-neutron interactions in terms of mass number A . Assuming these proton-neutron interactions, we predict atomic masses of nuclei in the transuranium region.

We now switch to the α -decay energies Q_α , defined by

$$Q_\alpha(Z, N) = M(Z, N) - M(Z - 2, N - 2) - M_{\text{He}}.$$

In Fig. 8, we present our predicted Q_α (in MeV) for nuclei with proton number Z from 90 to 106, with results of even- Z nuclei in Fig. 8(a) and those of odd- Z nuclei in Fig. 8(b). One sees our results are in very good agreement with experimental data except for three nuclei: ^{263}Sg and $^{256,257}\text{Db}$. The deviations of our predicted Q_α from experimental data are $0.3 \sim 0.4$ MeV in these three exceptional cases.

Similar to Refs. [14,69], we use the Viola-Seaborg formula [70]

$$\log_{10} T_\alpha = (aZ + b)Q_\alpha^{-1/2} + (cZ + d) + h_{\log}, \quad (5)$$

to evaluate α -decay half-lives T_α . Here $a = 1.64062$, $b = -8.54399$, $c = -0.19430$, and $d = -33.9054$. The hindrance factors h_{\log} are 0, 0.8937, 0.5720, and 0.9380 for the nuclei with (even Z , even N), (even Z , odd N), (odd Z , even N), and (odd Z , odd N), respectively.

In Table V, we compare our predicted results with previous studies, for Q_α (in MeV) and T_α (in s) of nuclei with proton number Z from 102 to 106 and neutron number near N around 152. ‘‘Cal-1, 2, 3’’ correspond to the results predicted in this work, Ref. [14], and Ref. [53], respectively. The experimental value of Q_α (Expt) are taken from Ref. [53]; T_α (Expt) are taken from [71] except for $^{255,257}\text{Rf}$, which are based on Refs. [72,73]. The values of Q_α in this work are close to experimental values or Audi’s predictions in Ref. [53]. Our $T_\alpha(\text{cal-1})$ reproduce the experimental values within a factor of 25.

C. Impact on astrophysical r -process simulations

The rapid neutron capture (r) process [74–77] was proposed half a century ago to explain the enrichment of elements heavier than iron in the universe. This process is believed to occur in an astrophysical environment of extremely high neutron intensity and high temperature, and to run along the very neutron-rich nuclei close to the drip line, most of which will be not accessible experimentally in the near future. A major source of the uncertainty in the r -process simulations

	64	66	68	70	72	74	76	78	80	82	84	86	88	90	92	94		
38	+5.16(16) +4.91(23) +6.70(18) +8.71(21)	+4.63(15) +4.46(45) +7.43(27) +7.66(45)	+4.17(21) +6.50(31) +5.66(35)	+3.88(28) +5.66(35) +4.94(39)	+3.65(20) +4.94(39) +4.36(41)	+3.61(29) +4.36(41) +3.40(43)	+3.07(21) +3.72(45) +3.40(43)	+3.05(32) +3.52(44) +3.69(46)	+3.16(32) +2.82(21) +3.52(44)	+2.82(21) +3.69(46) +3.72(45)	+0.33(35) +0.54(37) -0.73(49)	+0.54(37) +0.11(24) -0.79(52)	+0.11(24) -0.23(37) -1.47(53)	-0.23(37) -0.46(36) -2.15(53)	-0.46(36) -2.79(52)	-0.99(26)	Sr	
37	+4.41(16) +4.50(29) +7.78(24) +7.90(24)	+3.95(22) +6.62(31) +5.88(34)	+3.49(18) +5.88(34) +4.83(38)	+3.17(28) +4.83(38) +4.08(42)	+2.88(31) +4.08(42) +3.55(44)	+2.86(21) +3.55(44) +3.04(46)	+2.39(33) +2.97(47) +3.04(46)	+2.41(22) +2.73(47) +2.97(47)	+2.48(22) +2.73(47) +2.83(48)	+2.07(35) +2.83(48) +2.83(48)	-0.35(23) -1.50(54) -1.50(54)	-0.13(24) -1.50(54) -2.14(55)	-0.53(39) -2.81(54) -2.14(55)	-0.93(24) -2.81(54) -3.43(56)	-1.09(24) -3.38(54)		Rb	
36	+4.20(22) +4.48(71) +6.80(29) +6.85(71)	+3.84(18) +5.74(35) +4.83(38)	+3.31(26) +4.83(38) +4.01(41)	+3.05(20) +4.83(38) +4.01(41)	+2.79(22) +3.26(44) +2.70(46)	+2.77(32) +3.26(44) +2.73(46)	+2.31(22) +2.23(48) +2.15(49)	+2.25(35) +2.23(48) +2.15(49)	+2.39(35) +2.00(49) +2.00(49)	+1.99(23) +2.08(50) +2.08(50)	-0.42(37) -2.30(53) -2.30(53)	-0.15(40) -2.23(55) -2.84(56)	-0.57(25) -3.43(56) -3.43(56)	-0.84(39)			Kr	
35	+3.45(18) +5.76(33)	+3.14(28) +4.84(38)	+2.63(20) +4.04(41)	+2.41(32) +3.22(44)	+2.10(34) +2.45(47)	+2.02(22) +1.86(49)	+1.60(36) +1.45(50)	+1.59(23) +1.42(51)	+1.78(23) +1.27(51)	+1.27(38) +1.27(52)	-1.18(24) -3.14(55)	-0.86(26) -3.03(57)	-1.27(42) -3.57(58)				Br	
34	+3.10(27) +4.85(37)	+2.93(20) +3.88(41)	+2.51(31) +3.19(44)	+2.25(22) +2.39(47)	+1.99(23) +1.67(49)	+1.93(36) +1.06(51)	+1.52(24) +0.62(52)	+1.49(38) +0.62(53)	+1.62(38) +0.47(53)	+1.21(25) +0.59(54)	-1.25(40) -3.95(57)	-0.92(42) -3.84(59)					Se	
33	+2.51(21) +4.03(41)	+2.23(32) +2.87(44)	+1.80(22) +2.31(47)	+1.61(36) +1.63(49)	+1.37(38) +0.89(52)	+1.24(24) +0.28(53)	+0.81(39) -0.20(54)	+0.80(25) -0.13(56)	+0.98(25) -0.24(55)	+0.57(40) -0.16(56)	-2.01(26) -4.76(59)	-1.71(27) -4.70(61)					As	
32	+2.30(32) +3.13(44)	+1.90(23) +1.99(47)	+1.59(34) +1.38(49)	+1.50(24) +0.80(52)	+1.21(25) +0.09(54)	+1.11(39) -0.48(55)	+0.72(26) -0.97(56)	+0.71(41) -0.94(57)	+0.89(40) -1.00(57)	+0.43(26) -0.92(58)	-2.03(42) -5.52(60)	-1.76(45) -5.53(62)					Ge	
31	+1.64(23) +2.27(47)	+1.35(36) +1.19(50)	+0.89(24) +0.39(52)	+0.84(39) -0.06(54)	+0.59(41) -0.65(56)	+0.50(26) -1.23(58)	+0.07(42) -1.73(59)	+0.01(27) -1.73(59)	+0.22(26) -1.73(59)	-0.21(43) -1.65(60)	-2.77(27) -6.30(62)						Ga	
30	+1.41(36) +1.29(50)	+1.14(25) +0.32(53)	+0.54(38) -0.47(54)	+0.63(26) -0.97(56)	+0.48(27) -1.45(58)	+0.33(42) -2.01(60)	-0.04(27) -2.47(60)	-0.09(43) -2.48(61)										Zn
29	+0.68(25) +0.42(52)	+0.52(40) -0.52(55)	+0.00(26) -1.25(57)	-0.02(43) -1.93(59)	-0.16(44) -2.28(61)	-0.28(27) -2.72(62)	-0.61(45) -3.19(62)											Cu

One-neutron drip line
for even neutron number

FIG. 7. (Color online) Same as Fig. 6 except for nuclei with even neutron numbers. The unit of S_n and S_{2n} is MeV.

is the nuclear physics inputs employed. Encouraged by the improved mass accuracy in this work, we investigate in this subsection the impact of our predictions on r -process simulations.

Toward that goal, we employ a site-independent approach developed based on the waiting-point approximation, namely, the assumption of $(n, \gamma) \rightleftharpoons (\gamma, n)$ equilibrium. This model is ideal for studying the sensitivity of nuclear physics input in astrophysical simulations, and furthermore has also been successfully applied to studies of r -process patterns for both the solar system and metal-poor stars (see, e.g., Refs. [78–80]).

Under the assumption of $(n, \gamma) \rightleftharpoons (\gamma, n)$ equilibrium, the abundance ratios of two isotopes are given by

$$\frac{Y(Z, A+1)}{Y(Z, A)} = n_n \left(\frac{h^2}{2\pi m_n \kappa T} \right)^{3/2} \frac{G(Z, A+1)}{2G(Z, A)} \times \left(\frac{A+1}{A} \right)^{3/2} \exp \left[\frac{S_n(Z, A+1)}{\kappa T} \right], \quad (6)$$

where $Y(Z, A)$ denotes the abundance of the nuclide (Z, A) , n_n is the neutron density, T is the temperature of astrophysical environment, S_n is the one-neutron separation energy, and $G(Z, A)$ is the partition function of nuclide (Z, A) . h , κ , and m_n are the Planck constant, Boltzmann constant, and atomic mass unit, respectively. The knowledge of neutron separation energies in the first-order approximation determines the r -process path. For more details about the above model, we refer the reader to Refs. [78,80].

Before we turn to the impact of our results on nucleosynthesis, it is suggestive to look at our predicted S_n . Among all predicted S_n of 6426 nuclei, about 1900 nuclei are relevant for the astrophysical r process, and about 50% of these relevant S_n are predicted with theoretical accuracies better than 200 keV. The differences between such S_n and the

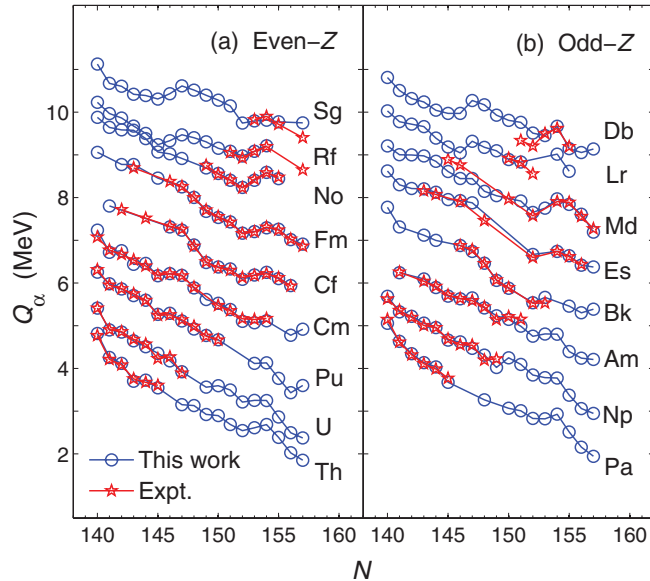


FIG. 8. (Color online) The α -decay energies Q_α (in MeV) for nuclei with proton number Z from 90 to 106. (a) Q_α for even- Z nuclei, (b) Q_α for odd- Z nuclei. Experimental data are based on the database of Ref. [53].

TABLE V. Predicted and experimental α -decay energies Q_α (in MeV) and half-lives T_α (in s) for nuclei with proton number $Z = 102$ to 106 and neutron number close to $N = 152$. “Cal-1,” “Cal-2,” and “Cal-3” represent the results of the present work, Ref. [14], and Audi’s predictions in Ref. [53], respectively. T_α (Cal-1,-2,-3) are obtained by the Viola-Seaborg formula. The experimental data Q_α (Expt) are obtained from Ref. [53]; T_α (Expt) are taken from [71] except those for $^{255,257}\text{Rf}$, which are taken from Refs. [72,73].

Nucl.	Q_α (Cal-1)	Q_α (Cal-2)	Q_α (Cal-3)	Q_α (Expt)	T_α (Cal-1)	T_α (Cal-2)	T_α (Cal-3)	T_α (Expt)
^{248}No	9.022		9.230		0.140		0.035	
^{249}No	8.916		9.170		2.252		0.410	
^{250}No		8.801	8.950			0.636	0.228	
^{251}No	8.696	8.643		8.751	10.498	15.3		0.916
^{252}No	8.567	8.493		8.549	3.398	5.84		≈ 3.64
^{253}No	8.406	8.290		8.414	87.326	0.21×10^3		
^{254}No	8.238	8.096		8.226	40.099	0.122×10^3		0.567×10^2
^{255}No	8.405	8.164		8.428	87.809	0.557×10^3		0.305×10^3
^{256}No	8.590	8.238		8.581	2.878	40.1		≈ 2.91
^{257}No	8.440	8.066		8.477	67.710	0.121×10^4		
^{251}Lr	9.177		9.534		0.413		0.041	
^{252}Lr	9.096		9.160		1.651		1.072	
^{253}Lr	8.892			8.918	2.874	2.50		0.644
^{254}Lr	8.831			8.816	10.233	23.7		17.105
^{255}Lr		8.521		8.556		41.4		25.882
^{256}Lr		8.595	8.811			55.5	11.783	31.765
^{257}Lr	9.017	8.714	9.008		1.214	10.1	1.296	≈ 0.646
^{258}Lr	8.616	8.545		8.910	47.808	80.3		4.1-4.32
^{259}Lr		8.383	8.584			1.160×10^2	26.006	7.949
^{253}Rf	9.304	9.522	9.550		0.830	0.202	0.169	$\approx 0.26 \times 10^{-1}$
^{254}Rf	9.154	9.336	9.210		0.288	0.855×10^{-1}	0.197	
^{255}Rf	9.081	9.140		9.055	3.694	2.47		3.154
^{256}Rf	8.977	8.952		8.925	0.961	1.14		2.016
^{257}Rf	9.080	9.071		9.083	3.701	3.95		5.34/4.43
^{258}Rf	9.213	9.195		9.193	0.194	0.219		0.923×10^{-1}
^{259}Rf		9.028	9.130			5.30	2.644	3.04
^{260}Rf		8.870	8.900			2.04	1.648	
^{261}Rf		8.702		8.648		53.2		
^{255}Db	9.808		9.420		0.035		0.406	
^{256}Db	9.762	9.550		9.336	0.108	0.408		2.5
^{257}Db	9.508	9.407		9.206	0.230	0.443		1.53 ~ 1.63
^{258}Db	9.451	9.529		9.501	0.772	0.465		7.03
^{259}Db	9.667	9.655		9.619	0.084	0.903×10^{-1}		0.51
^{260}Db	9.144	9.494		9.192	5.946	0.585		1.52 ~ 1.68
^{261}Db	9.054	9.337	9.218		4.752	0.699	1.547	1.8 ~ 2.20
^{262}Db	9.136		9.008		6.282		15.041	
^{256}Sg	10.282				0.120×10^{-2}			
^{257}Sg	10.145				0.204×10^{-1}			
^{258}Sg	9.743	9.867	9.670		0.300×10^{-1}	0.139×10^{-1}	0.473×10^{-1}	$> 0.165 \times 10^{-1}$
^{259}Sg	9.794	9.991		9.821	0.171	0.509×10^{-1}		0.644
^{260}Sg	9.813	10.121		9.900	0.193×10^{-1}	0.301×10^{-2}		0.95×10^{-2}
^{261}Sg	9.773	9.961		9.714	0.194	0.611×10^{-1}		≈ 0.23
^{262}Sg		9.810	9.600			0.197×10^{-1}	0.739×10^{-1}	$> 0.364 \times 10^{-1}$
^{263}Sg	9.751	9.648		9.403	0.223	0.428		1.0 ~ 1.43

corresponding results of the Duflo-Zuker model [4,5] are shown in Fig. 9. One sees notable differences around the neutron magic number $N = 126$. More precisely, a relatively smoother evolution of S_n toward the one-neutron drip line for nuclei with $N \sim 126$ is predicted in this work [also see Fig. 5(d) for the Tm isotopes]. A similar trend also holds when comparing with the FRDM model. Unquestionably, the differ-

ences are rooted in the long-range extrapolation of the shell effect.

To illustrate the influence of our predicted S_n values on the abundance of r -process nuclei, two simulations based on different mass sets are performed under an astrophysical condition with a constant neutron density of 10^{26} cm^{-3} and a constant temperature of $1.5 \times 10^9 \text{ K}$. In both simulations,

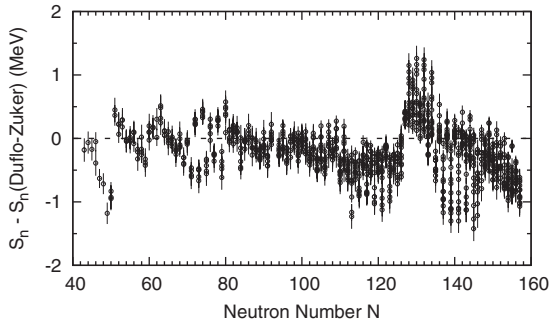


FIG. 9. Difference between one-neutron separation energies predicted in this work and those in Duflo-Zuker model. In this comparison, the corresponding separation energies are computed in our approach with theoretical accuracies better than 200 keV.

the neutron irradiation time is fixed to 1.4 s. We note that the astrophysical condition here is chosen to highlight the nuclear mass impact in the resulting abundance curves, not to reproduce the whole solar r -process distribution. The results normalized to the solar- r -process abundance (empty circles) at $A = 130$ are shown in Fig. 10. The blue-dashed curve (marked by Duflo-Zuker) represents the result using the Duflo-Zuker mass model [4,5]. The red-solid curve (marked by Duflo-Zuker*) is the same as the blue-dashed one except that we replace the corresponding Duflo-Zuker data by our predicted S_n with theoretical errors below 200 keV. The solar r -process abundances [81] are also displayed for comparison.

In Fig. 10 one sees that, under the above astrophysical condition, both simulations present similar results for mass number less than 170. This is determined by the almost identical r -process paths in this range. Furthermore, both cases can reproduce generally the second and third abundance peaks at $A \sim 130$ and 195 in the solar r -process abundance curve. However, they differ significantly in the absolute values around the third peak in Fig. 10, where the abundances in the hybrid case are reduced by more than one order of magnitude in comparison with the Duflo-Zuker case. This discrepancy can

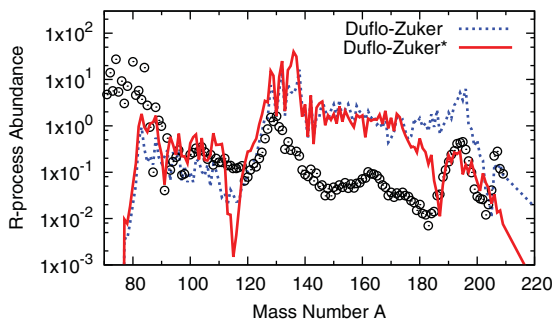


FIG. 10. (Color online) r -process simulations (on a logarithmic scale) calculated by using two mass sets (Duflo-Zuker and Duflo-Zuker*) under an astrophysical condition with a constant neutron density of 10^{26} cm^{-3} and a constant temperature of $1.5 \times 10^9 \text{ K}$. The neutron irradiation time in both simulations is fixed to 1.4 s. The calculated values are normalized to the solar r -process abundance (empty circles) at $A = 130$.

be easily traced back to the S_n differences around $N = 126$ in the two models as shown in Figs. 5(d) and 9. A smoother evolution of S_n toward the neutron drip line for nuclei heavier than Nd would result in two effects. First, the r -process path runs about 1 to 3 atomic mass units closer to the stability line (i.e., to nuclei with longer β -decay lifetime) when approaching nuclei with $N = 126$. This eventually leads to a sharp drop in abundances before the third peak, since the abundance flowing from one isotopic chain to the next is governed by β decays. Second, less materials are accumulated into the nuclei with $N = 126$, which results in a less-pronounced peak compared with the Duflo-Zuker case. Meanwhile, we notice that, by using our predictions, the overall shape and position of the third r -process abundance peaks can be better reproduced.

IV. SUMMARY AND CONCLUSIONS

In this paper we improve the accuracy of the description and prediction of atomic masses by manipulating local mass relations which connect with the proton-neutron (p - n) interactions. Instead of considering various corrections simultaneously in the evaluation of the proton-neutron interactions, we focus on the shell correction (which is the dominant correction among all) and optimize this term for different shells. The uncertainties of our predicted results are reduced substantially for nuclei with mass number $A \leq 120$. Some of the previously predicted results which exhibit large deviations [30] from the experimental database are now satisfactorily obtained (see Fig. 1).

We discuss a few issues of interests by using our predicted atomic masses: (1) We evaluate the separation energies for one- and two-proton (neutron) emissions. In comparison with experimental database, the rmsDs of our predicted B^{pred} , S_p^{pred} , S_n^{pred} , S_{2p}^{pred} , and S_{2n}^{pred} with respect to experimental data are improved to 89, 106, 112, 140, and 126 keV, respectively, for nuclei with $A \geq 60$. We predict proton and neutron drip lines for a number of regions in the nuclide chart and compare them with several theoretical models. (2) We investigate α -decay energies (Q_α) of transuranium nuclei. For experimentally known Q_α , the rmsD of our predictions is only ~ 50 keV (although a very few cases have rmsD ~ 0.3 to 0.4 MeV). By using our predicted α -decay energies, we evaluate α -decay lifetimes of these nuclei. (3) We investigate the nuclear mass impact on the astrophysical r -process nucleosynthesis. By using our predicted S_n (with theoretical errors below 200 keV), the overall shape and position of the third r -process abundance peaks can be better reproduced under the given conditions in comparison with the Duflo-Zuker database [4,5], and a significant difference in abundances arises after mass number 170.

ACKNOWLEDGMENTS

The authors would like to thank Professor S. W. Xu for discussions and Professor Y. Z. Qian for his reading of this paper. We thank the National Natural Science Foundation of China for supporting this work under Grants No. 10975072, No.10975096, No. 10975192, No. 10979074, No. 11128510, No. 11035001, No.11145005, No.11105010, No.11035007, and No. 11120101005. This work is also supported by the

Science & Technology Committee of Shanghai city under Grant No. 11DZ2260700, and the Science & Technology Program of Shanghai Maritime University under Grant No. 20100086. BS is also partially supported by NCET-09-0031 and the Fundamental Research Funds for the Central Universities.

APPENDIX: FORMULAS OF PREDICTING ONE- AND TWO-NUCLEON SEPARATION ENERGIES

In this appendix we present the formulas of evaluating S_p , S_n , S_{2p} , and S_{2n} . As for the formulas of predicting binding energies, see Eqs. (9) and (10) of Ref. [30].

$$S_p^{\text{pred}}(Z, N) = S_p(Z, N - 1) + \delta V_{1p-1n}^{\text{cal}}(Z, N),$$

$$S_p^{\text{pred}}(Z, N) = S_p(Z, N + 1) - \delta V_{1p-1n}^{\text{cal}}(Z, N + 1),$$

$$S_p^{\text{pred}}(Z, N) = S_p(Z, N - 2) + \delta V_{1p-2n}^{\text{cal}}(Z, N),$$

$$S_p^{\text{pred}}(Z, N) = S_p(Z, N + 2) - \delta V_{1p-2n}^{\text{cal}}(Z, N + 2),$$

$$S_n^{\text{pred}}(Z, N) = S_n(Z - 1, N) + \delta V_{1p-1n}^{\text{cal}}(Z, N),$$

$$S_n^{\text{pred}}(Z, N) = S_n(Z + 1, N) - \delta V_{1p-1n}^{\text{cal}}(Z + 1, N),$$

$$S_n^{\text{pred}}(Z, N) = S_n(Z - 2, N) + \delta V_{2p-1n}^{\text{cal}}(Z, N),$$

$$S_n^{\text{pred}}(Z, N) = S_n(Z + 2, N) - \delta V_{2p-1n}^{\text{cal}}(Z + 2, N),$$

$$S_{2p}^{\text{pred}}(Z, N) = S_{2p}(Z, N - 1) + \delta V_{2p-1n}^{\text{cal}}(Z, N),$$

$$S_{2p}^{\text{pred}}(Z, N) = S_{2p}(Z, N + 1) - \delta V_{2p-1n}^{\text{cal}}(Z, N + 1),$$

$$S_{2n}^{\text{pred}}(Z, N) = S_{2n}(Z - 1, N) + \delta V_{1p-2n}^{\text{cal}}(Z, N),$$

$$S_{2n}^{\text{pred}}(Z, N) = S_{2n}(Z + 1, N) - \delta V_{1p-2n}^{\text{cal}}(Z + 1, N).$$

-
- [1] C. F. von Weizsäcker, *Z. Phys.* **96**, 431 (1935).
 [2] H. A. Bethe and R. F. Bacher, *Rev. Mod. Phys.* **8**, 82 (1936).
 [3] W. D. Myers and W. J. Swiatecki, *Nucl. Phys.* **81**, 1 (1966).
 [4] J. Duflo and A. P. Zuker, *Phys. Rev. C* **52**, R23 (1995).
 [5] J. Duflo and A. P. Zuker, [<http://amdc.in2p3.fr/web/dz.html>].
 [6] P. Möller, J. R. Nix, W. D. Myers, and W. J. Swiatecki, *At. Data Nucl. Data Tables* **59**, 185 (1995).
 [7] P. Möller, W. D. Myers, H. Sagawa, and S. Yoshida, *Phys. Rev. Lett.* **108**, 052501 (2012).
 [8] S. Goriely, F. Tondeur, and J. M. Pearson, *At. Data Nucl. Data Tables* **77**, 311 (2001).
 [9] S. Goriely, N. Chamel, and J. M. Pearson, *Phys. Rev. C* **82**, 035804 (2010).
 [10] L. S. Geng, H. Toki, and J. Meng, *Prog. Theor. Phys.* **113**, 785 (2005).
 [11] N. Wang, M. Liu, and X. Z. Wu, *Phys. Rev. C* **81**, 044322 (2010).
 [12] M. Liu, N. Wang, Y. Deng, and X. Wu, *Phys. Rev. C* **84**, 014333 (2011).
 [13] N. Wang and M. Liu, *Phys. Rev. C* **84**, 051303(R) (2011).
 [14] T. K. Dong and Z. Z. Ren, *Phys. Rev. C* **72**, 064331 (2005); **77**, 064310 (2008).
 [15] A. Bhagwat, X. Viñas, M. Centelles, P. Schuck, and R. Wyss, *Phys. Rev. C* **81**, 044321 (2010).
 [16] M. Bertolli, T. Papenbrock, and S. M. Wild, *Phys. Rev. C* **85**, 014322 (2012).
 [17] G. Audi and A. H. Wapstra, *Nucl. Phys. A* **565**, 1 (1993).
 [18] G. Audi and A. H. Wapstra, *Nucl. Phys. A* **595**, 409 (1995).
 [19] G. Audi, A. H. Wapstra, and C. Thibault, *Nucl. Phys. A* **729**, 337 (2003); [<http://www.nndc.bnl.gov/masses/mass.mas03>].
 [20] G. T. Garvey and I. Kelson, *Phys. Rev. Lett.* **16**, 197 (1966); G. T. Garvey, W. J. Gerace, R. L. Jaffe, I. Talmi, and I. Kelson, *Rev. Mod. Phys.* **41**, S1 (1969).
 [21] J. Janecke and H. Behrens, *Phys. Rev. C* **9**, 1276 (1974).
 [22] J. E. Monahan and F. J. D. Serduke, *Phys. Rev. C* **15**, 1080 (1977); **17**, 1196 (1978).
 [23] J. Janecke and P. Masson, *Phys. Rev. C* **32**, 1390 (1985).
 [24] J. Barea, A. Frank, J. G. Hirsch, and P. Van Isacker, *Phys. Rev. Lett.* **94**, 102501 (2005).
 [25] J. Barea, A. Frank, J. G. Hirsch, P. Van Isacker, S. Pittel, and V. Velázquez, *Phys. Rev. C* **77**, 041304 (2008).
 [26] J. G. Hirsch, I. Morales, J. Mendoza-Temis, A. Frank, J. C. Lopez-Vieyra, J. Barea, A. Frank, S. Pittel, P. Van Isacker, and V. Velázquez, *Int. J. Mod. Phys. E* **17**, 398 (2008).
 [27] I. O. Morales and A. Frank, *Phys. Rev. C* **83**, 054309 (2011).
 [28] G. J. Fu, H. Jiang, Y. M. Zhao, S. Pittel, and A. Arima, *Phys. Rev. C* **82**, 034304 (2010).
 [29] H. Jiang, G. J. Fu, Y. M. Zhao, and A. Arima, *Phys. Rev. C* **82**, 054317 (2010).
 [30] G. J. Fu, Y. Lei, H. Jiang, Y. M. Zhao, B. Sun, and A. Arima, *Phys. Rev. C* **84**, 034311 (2011).
 [31] D. Lunney, J. M. Pearson, and C. Thibault, *Rev. Mod. Phys.* **75**, 1021 (2003).
 [32] K. Blaum, *Phys. Rep.* **425**, 1 (2006).
 [33] A. de Shalit and M. Goldhaber, *Phys. Rev.* **92**, 1211 (1953).
 [34] I. Talmi, *Rev. Mod. Phys.* **34**, 704 (1962).
 [35] P. Federman and S. Pittel, *Phys. Lett. B* **69**, 385 (1977); **77**, 29 (1978); *Phys. Rev. C* **20**, 820 (1979).
 [36] R. F. Casten, *Nucl. Phys. A* **443**, 1 (1985); *Phys. Rev. Lett.* **54**, 1991 (1985).
 [37] R. F. Casten and N. V. Zamfir, *J. Phys. G* **22**, 1521 (1996).
 [38] M. K. Basu and D. Banerjee, *Phys. Rev. C* **3**, 992 (1971); **4**, 652 (1971).
 [39] J. Janecke, *Phys. Rev. C* **6**, 467 (1972).
 [40] J. Y. Zhang, C. S. Wu, C. H. Yu and J. D. Garrett, Proc. Int. Conf. on Contemporary Topics in Nuclear Structure, Cocoyoc, Mexico, Book of Abstracts **C 65**, 109 (1988) (unpublished).
 [41] J. Y. Zhang, R. F. Casten, and D. S. Brenner, *Phys. Lett. B* **227**, 1 (1989).
 [42] D. S. Brenner, C. Wesselborg, R. F. Casten, D. D. Warner, and J. Y. Zhang, *Phys. Lett. B* **243**, 1 (1990).
 [43] Z. C. Gao and Y. S. Chen, *Phys. Rev. C* **59**, 735 (1999); Z. C. Gao, Y. S. Chen, and J. Meng, *Chin. Phys. Lett.* **18**, 1186 (2001).
 [44] G. Mouze and C. Ythier, *Nuovo Cimento A* **103**, 105 (1990); **103**, 131 (1990); **103**, 1467 (1990); G. Mouze, S. Bidegainberry, A. Rocaboy, and C. Ythier, *ibid.* **106**, 885 (1993); G. Mouze, *ibid.* **107**, 1565 (1994); G. Mouze and A. Rocaboy, *ibid.* **109**, 527 (1996).

- [45] P. Van Isacker, D. D. Warner, and D. S. Brenner, *Phys. Rev. Lett.* **74**, 4607 (1995).
- [46] R. B. Cakirli, D. S. Brenner, R. F. Casten, and E. A. Millman, *Phys. Rev. Lett.* **94**, 092501 (2005).
- [47] R. B. Cakirli and R. F. Casten, *Phys. Rev. Lett.* **96**, 132501 (2006).
- [48] D. S. Brenner, R. B. Cakirli, and R. F. Casten, *Phys. Rev. C* **73**, 034315 (2006).
- [49] Y. Oktem, R. B. Cakirli, R. F. Casten, R. J. Casperson, and D. S. Brenner, *Phys. Rev. C* **74**, 027304 (2006).
- [50] M. Stoitsov, R. B. Cakirli, R. F. Casten, W. Nazarewicz, and W. Satula, *Phys. Rev. Lett.* **98**, 132502 (2007).
- [51] M. Breitenfeldt *et al.*, *Phys. Rev. C* **81**, 034313 (2010).
- [52] R. B. Cakirli, K. Blaum, and R. F. Casten, *Phys. Rev. C* **82**, 061304(R) (2010).
- [53] G. Audi and M. Wang (private communication).
- [54] E. Haettner *et al.*, *Phys. Rev. Lett.* **106**, 122501 (2011).
- [55] C. Weber *et al.*, *Phys. Rev. C* **78**, 054310 (2008).
- [56] B. Sun *et al.*, *Nucl. Phys. A* **812**, 1 (2008).
- [57] D. Neidherr *et al.*, *Phys. Rev. Lett.* **102**, 112501 (2009).
- [58] L. Chen, Ph.D. thesis, Justus-Liebig-University Giessen, 2008; L. Chen *et al.*, *Nucl. Phys. A* **882**, 71 (2012).
- [59] L. Chen *et al.*, *Phys. Lett. B* **691**, 234 (2010).
- [60] B. A. Brown, R. R. C. Clement, H. Schatz, A. Volya, and W. A. Richter, *Phys. Rev. C* **65**, 045802 (2002).
- [61] B. H. Sun, P. W. Zhao, and J. Meng, *Sci. China Phys. Mech. Astron.* **54**, 210 (2011).
- [62] G. A. Lalazissis, D. Vretenar, and P. Ring, *Phys. Rev. C* **69**, 017301 (2004).
- [63] A. Kankainen *et al.*, *Eur. Phys. J. A* **29**, 271 (2006).
- [64] H. Jiang, G. J. Fu, Y. M. Zhao, and A. Arima, *Phys. Rev. C* **85**, 024301 (2012).
- [65] B. Blank *et al.*, *Phys. Rev. Lett.* **94**, 0232501 (2005).
- [66] P. Ascher *et al.*, *Phys. Rev. Lett.* **107**, 102502 (2011).
- [67] S. Q. Zhang, J. Meng, and S. G. Zhou, *Science in China Series G* **46**, 632 (2003).
- [68] M. Bhattacharya and G. Gangopadhyay, *Phys. Rev. C* **72**, 044318 (2005).
- [69] T. K. Dong and Z. Z. Ren, *Eur. Phys. J. A* **26**, 69 (2005).
- [70] V. E. Viola and G. T. Seaborg, *J. Inorg. Nucl. Chem.* **28**, 741 (1966).
- [71] G. Audi, O. Bersillon, J. Blachot, and A. H. Wapstra, *Nucl. Phys. A* **729**, 3 (2003).
- [72] J. K. Tuli, S. Singh, and A. K. Jain, *Nucl. Data Sheets* **107**, 1347 (2006).
- [73] A. K. Jain, S. Singh, and J. K. Tuli, *Nucl. Data Sheets* **107**, 2103 (2006).
- [74] E. M. Burbidge, G. R. Burbidge, W. A. Fowler, and F. Hoyle, *Rev. Mod. Phys.* **29**, 547 (1957).
- [75] J. J. Cowan, F. K. Thieleman, and J. W. Truran, *Phys. Rep.* **208**, 267 (1991).
- [76] Y. Z. Qian, *Prog. Part. Nucl. Phys.* **50**, 153 (2003).
- [77] M. Arnould, S. Goriely, and K. Takahashi, *Phys. Rep.* **450**, 97 (2007).
- [78] B. Sun, F. Montes, L. S. Geng, H. Geissel, Y. A. Litvinov, and J. Meng, *Phys. Rev. C* **78**, 025806 (2008).
- [79] B. Sun and J. Meng, *Chin. Phys. Lett.* **25**, 2429 (2008).
- [80] Z. M. Niu, B. Sun, and J. Meng, *Phys. Rev. C* **80**, 065806 (2009).
- [81] C. Sneden, J. J. Cowan, and R. Gallino, *Annu. Rev. Astron. Astrophys.* **46**, 241 (2008).